Nuclear Instruments and Methods in Physics Research B 557 (2024) 165532

Contents lists available at ScienceDirect

Nuclear Inst. and Methods in Physics Research, B

journal homepage: www.elsevier.com/locate/nimb

Full length article

The use of second foil stripping in tandem accelerators

T.L. Bailey *, L.K. Callahan, A.M. Clark, A.D. Nelson, L. Wood, P. Collon

Department of Physics and Astronomy, University of Notre Dame, Notre Dame, IN, 46556, USA

ARTICLE INFO

Keywords:
Electrostatic accelerators
Foil strippers
Accelerator mass spectrometry
AMS
Charge states

ABSTRACT

The 10 MV FN Tandem at the University of Notre Dame's Nuclear Science Laboratory has the option for a second foil stripper halfway down its high energy column. With its utilization, users are able to produce beams with higher energies and/or transmission than single foil stripping alone would be capable of achieving. A discussion of the Schiwietz–Grande, Nikolaev–Dmitriev, and Baudinet-Robinet semi-empirical models used to determine the resulting charge state abundances, as well as how they compare to measured charge state distributions is presented. The advantages of a second foil stripper are discussed alongside measurements of the charge state abundances produced. The potential for more interfering beam species of similar magnetic rigidity is also discussed. It was found that for most of the beams tested, second foil stripping allowed higher energies with higher yields than the single terminal foil stripping alone could achieve which can enhance the capabilities of other laboratories using similar accelerator systems.

1. Introduction

Electrostatic tandem accelerators in the range of 3–14 MV are in use worldwide for low energy nuclear physics research [1]. Applications of these devices range from fundamental research probing the standard model, to a wide array of analytical techniques. Despite the many different types and sizes, each device follows the same basic principles. First, a negatively charged beam is accelerated from ground to a positive terminal. There, the beam is stripped of a number of electrons. Finally, the positively charged beam is repelled from the terminal down the beamline and into the experimental setups. The energy of this beam is given by

$$E = TV \times \left(\frac{m_e}{m_i} + q\right) + E_i \frac{m_e}{m_i} \tag{1}$$

where m_i and m_e are the mass of the injected molecule and extracted positive ion, q is the selected charge state, TV is the Terminal Voltage and E_i is the energy of the injected molecule provided by the ion source. Typically, gas in the stripping canal, and/or a carbon foil is used to strip electrons inside the terminal [2]. Additionally, an added benefit to the electron stripping is that injected molecules are dissociated as a part of this process. A feature of the University of Notre Dame's 10 MV FN tandem accelerator is the optional second foil stripper halfway down the high energy column [3] as shown in Fig. 1 providing a beam energy of

$$E = TV \times \left(\frac{m_e}{m_i} + \frac{q_1 + q_2}{2}\right) + E_i \frac{m_e}{m_i} \tag{2}$$

where q_1 and q_2 represent the charge states selected at the terminal and second foil stripper, respectively. The additional velocity gained between the two stripper foils results in higher charge states and energies than single foil stripping alone is capable of achieving [2,4], providing many benefits. Of the many tandem accelerators in existence, very few (~15) are capable of reaching a terminal voltage of ≥10 MV such as the FN Tandem at the University of Notre Dame. Nearly double that amount can reach ≥6 MV [1], which, with a second foil stripper, would be able to reach energies previously unattainable with terminal foil stripping alone. The larger amount of ≥6 MV machines worldwide prompted the selection of the energy range of this paper. Despite their advantages, there exists little characterization of the capabilities of such a system.

The primary benefit of the second foil stripper is the capability to produce beams with a higher total energy. The energy gained from accelerating the higher charge states can enable researchers to scan through higher energy resonances in nuclear reactions, or limit the dispersion of desired radioactive ion beams generated in-flight. The second foil stripper can also yield high energy beams with better transmission, especially when the higher energy necessitates the selection of an unfavorable charge state using only single foil stripping. In measurements where the total current delivered is critical to limiting long counting times, a second foil stripper can be crucial to acquiring sufficient data in a reasonable time.

These benefits are not without additional challenges however. The extra foil stripper gives multiple paths to the same energy beam and significantly increases the likelihood of other E/q and p/q interferences.

* Corresponding author.
E-mail address: tbailey3@nd.edu (T.L. Bailey).

https://doi.org/10.1016/j.nimb.2024.165532
Received 12 January 2024; Received in revised form 6 September 2024; Accepted 13 September 2024
Available online 25 September 2024

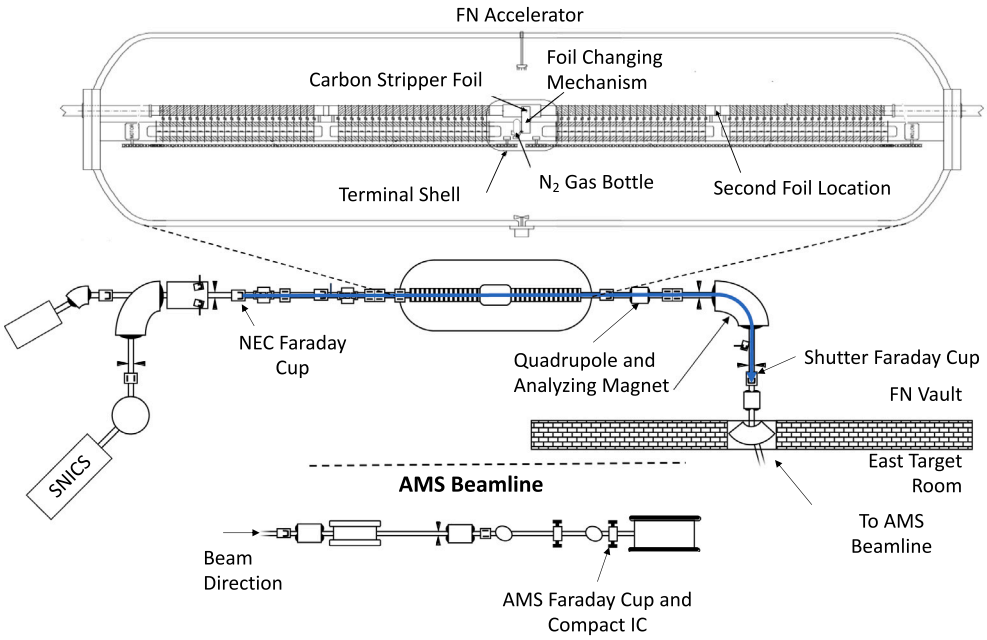

Fig. 1. Schematic for the FN Tandem Accelerator and associated components at the NSL. At the top is the accelerator, with locations of the different strippers shown. The middle section indicates the points between which the transmission is measured using a blue line. The quadrupole, analyzing magnet, and shutter Faraday cup are also pointed out. The bottom of the figure shows the AMS beamline, used to identify all species present in each beam.

The post-acceleration magnet that is standard at electrostatic accelerator facilities can filter out E/q contaminants, but fails to eliminate p/q interferences necessitating further filtering. The emission of electrons and ions from the second foil stripper can cause issues described in detail in [2]. Without sufficient suppression, the electrons will produce a large X-ray flux which can lower the insulation provided by gas in the accelerator tank. The ions will hit the acceleration tube, creating additional X-rays, and electrons that lead to loading. This can cause the electric potential at the second foil stripper to lower, requiring compensation at the terminal in order to maintain a constant energy. If running at the limits of the accelerator's capabilities, the beam loading could lead to excessive sparks as the machine tries to maintain a constant energy output. Another issue is the possibility of the foil to fail. When this occurs, if significant loading is present, a rapid increase of the terminal voltage may occur leading to damaging sparks. This is less of a concern however as the second foil stripper will generally have a much longer lifetime as the faster beam causes less radiation damage [2]. Another consideration is the angular straggling in the second foil stripper, increasing the beam's emittance and decreasing the overall transmission as more beam is scattered away. Empirically, the mean square scattering angle can be given by

$$\langle \phi^2 \rangle = 0.25\Big(\frac{Z_s(Z_s+1)}{A_s}\Big)\frac{Z_i^2}{E_i^2}L \tag{3}$$

where L, Z_s, and A_s are the thickness, proton number, and atomic number of the stripper foil, and Z_i and E_i are the proton number and energy of the ion [5]. Since the energy of the beam is much higher at the second foil stripper, the contribution to the emittance is lower. It is expected that there will be additional losses from the second foil stripper, but that fraction should be lower than what was lost from scattering at the terminal foil stripper.

The benefits for Accelerator Mass Spectrometry (AMS) of the second foil stripper in the accelerator itself have been identified previously at the University of Notre Dame's Nuclear Science Laboratory (NSL) [3,6], however the advantages provided by it are not exclusive to AMS measurements, and have found applications in numerous other accelerator based nuclear physics experiments, i.e. cross section measurements and radioactive ion beams. This has prompted further investigation into its capabilities for a host of nuclear physics related experiments.

2. Charge state predictions

The final charge state of an atom that passes through a stripping medium can vary due to multiple electron exchange interactions taking place. Analytical solutions for these various charge states may be possible for the lightest ion beams, however, for heavier elements, an empirical model is needed to predict the resulting charge state distributions [7]. Many such models exist, including some of the first ones from Bohr [7], as well as some that are used more frequently today such as Ziegler–Biersack–Littmark [8] used in the well known SRIM code, and Sayer [9]. One of the more recent, and well known models was developed by Schiewitz and Grande (SG) and is the one that will be used to predict charge abundances for this work. Predictions vary by model, and the choice of SG is one of many that can be taken for the purposes of this work.

The SG model was developed by using a multi-parameter least squares fit for 840 published data points representing a wide array of beams [10]. A further adjustment to the model, described in [11] gives the mean charge state formula as

$$\bar{q} = Z_p\frac{8.29x + x^4}{0.06/x + 4 + 7.4x + 10.37x + x^4} \tag{4}$$

with

$$x = c_1(\tilde{v}/c_2/1.54)^{1+1.83/Z_p} \tag{5}$$

$$c_1 = 1 - 0.26e^{-Z_t/11}e^{-\frac{(Z_t-Z_p)^2}{9}} \tag{6}$$

$$c_2 = 1 + 0.030\tilde{v}\ln(Z_t) \tag{7}$$

$$\tilde{v} = Z_p^{-0.543}v_p/v_0 \tag{8}$$

where Z_p and Z_t correspond to the projectile and target atomic numbers (beam and stripper foil), v_0 is the Bohr velocity of 2.19×10^6 m/s, and v_p is the atom's velocity at the terminal and second foil stripper. Taking the mean charge state into account, the width d of the distribution is given by Nikolaev and Dmitriev [12] as

$$d = \frac{1}{2}\sqrt{Z_p}\left(1 + X^{-5/3}\right)^{-4/5}X^{-5/6} \tag{9}$$

where $X = 0.608v_p/(Z^{0.45}v_0)$ represents a reduced velocity term [12, 13].

The shape of the distribution is predicted following the work of Baudinet-Robinet [14] who originally used the mean charge state formula put forth by To and Drouin [15]. Baudinet-Robinet uses a reduced chi-square model with the parameters

$$F(q;v) = \frac{ct^{\frac{v}{2}-1}e^{-t/2}}{2^{v/2}\Gamma(v/2)}$$
$$t = c(Z+2-q) \quad (10)$$
$$v = 2(Z+2-\bar{q})^2/d^2$$
$$c = 2(Z+2-\bar{q})/d^2$$

with Γ being the gamma function. Using the mean charge state given by Schiwietz and Grande, the distribution width given by Nikolaev and Dmitriev, and the distribution shape given by Baudinet-Robinet, a combination of Eqs. (4), (9) and (10) is used to predict the charge state abundances using both single and second foil stripping.

There still exists limitations of the SG model based on the datasets used, however the SG model is the most encompassing semi-empirical model, with the fits determined based on experimental data for beams of Z_p in the range 1–92 and stripper foils of Z_t in the range of 4–83 [10] over a finite range of beam energies. For ions heavier than Helium, the SG model considers energies where $v_p/v_0 \geq 0.4$ [11], which is true for all beams presented in this work, thus the model provides a valid prediction for expected charge state distributions.

3. Methods

The NSL is equipped with an MC-SNICS ion source used to produce all of the beams in this work. Beams of aluminum, manganese, iron, and zirconium were produced, chosen for the ease of production, relevance to ongoing AMS projects, and to cover beams injected elementally or as a molecule.

Each negative beam was accelerated to the terminal held at 6 MV with the exception of one of the measurements of the Aluminum beam at 3 MV. 6 MV was chosen since it is an attainable voltage at many tandem electrostatic accelerators [1]. The beams pass through a carbon foil and are accelerated to the high energy side. Halfway down the high energy column, at a potential of $TV/2.02$, is the second foil stripper where another carbon foil can sit. Both foils are 3.0(3) $\mu g/cm^2$ and are sourced from Arizona Carbon Foils. A quadrupole doublet focuses the beam and an analyzing magnet selects the appropriate charge state that is then ultimately measured on the shutter Faraday cup, described in detail in [16]. While scanning through charge states, the quadrupole and analyzing magnet are scaled together to keep different charge states from having different beam optics. Single foil stripping charge state abundances were measured until there was no readable current at a given high or low charge state. Once the single foil stripping measurements were taken, the second foil stripper was cycled in and the resulting charge state distribution was measured. These measurements occurred over a 12 h period. During this time, no degradation of the second stripper foils was observed. There were also no observable effects of beam loading as the terminal voltage was maintained using its generating voltmeter rather than relying on the analyzing slits feedback system.

In all measurements, the most abundant beam, based on model predictions, was developed first before bringing the magnetic elements up to the highest field strength corresponding to a likely charge state combination. This was done to limit hysteresis effects. The predicted abundant charge states were then measured in order of decreasing magnetic rigidity. Based on observations made, a second pass was performed by bringing the magnets up again and scanning down in rigidity to measure the lowest occupied states that could be measured on the Faraday cup.

Throughout the process, each beam was sent down the AMS beamline at the NSL to determine the number of distinct species in the beam. In addition to the existing quadrupole doublet and analyzing magnet, three more quadrupoles and a beamline selecting magnet were used. The AMS beamline is equipped with a silicon detector and retractable compact ionization chamber, described in [17] that is used to determine how many beam species with similar magnetic rigidity pass through the analyzing magnet as well as what fraction of the beam they account for such that corrections could be made for current measurements. In order to see all species, the beamline's Wien filter was not used. Particle identification is done using the compact ionization chamber. For each charge state selected, the ratio of counts identified to be the ion of interest, and total counts is used to make a correction to the particle transmission.

The total transmission through the accelerator system was also determined following the equations

$$\varepsilon_S = \sum_i \frac{I_{S,i}}{q_i I_{NEC}} \quad (11)$$

$$\varepsilon_D = \sum_{i,j} \frac{I_{S,ij}}{q_j I_{NEC}} \quad (12)$$

with $I_{S,i}$ and $I_{S,ij}$ representing the current measured on the shutter Faraday Cup, I_{NEC} representing the current on the NEC Faraday Cup (both shown in Fig. 1), q_i is the charge state after the terminal foil stripper, q_j is the charge state after the second foil stripper, and the bounds of summation are determined by the detectable current limit in the shutter Faraday Cup. ε_S and ε_D are the total transmissions when using single foil stripping and double foil stripping, respectively. The values for ε_S and ε_D are given in Table 1, and used to normalize the results displayed in Figs. 2–4. In order to characterize the difference in scattering losses through each foil stripper, the ratio of transmissions is defined as

$$R_T = \frac{\varepsilon_S}{\varepsilon_D/\varepsilon_S} \quad (13)$$

with ε_S and ε_D defined in Eqs. (11) and (12). The fraction $\varepsilon_D/\varepsilon_S$ is the total transmission through the second foil stripper alone. R_T compares the scattering losses at each foil stripper with values < 1 corresponding to less scattering losses at the second foil stripper.

The uncertainty of the Faraday cup measurements was 5% except for beams measured below 1 electrical nA, in which case 10% was used. Not all states were able to be measured due to their low abundances. The effect that these have are minimal though when considering their neighboring states are already a few orders of magnitude below the maxima, with the exception of the zirconium beam. The zirconium case was also limited by the magnetic rigidity, thus any state below 6+ was not measured.

4. Results

4.1. Single foil stripping results

The single foil stripping charge state distribution of four different isotopes were measured. The results are shown in Table 1 and the distributions are shown in Fig. 2. The total transmissions were generally lower than those measured by other facilities [18,19], in part due to the FN being operated at 6 MV as opposed to closer to its maximum value. An additional constraint is the gas stripping canal. The NSL's FN is still equipped with its original stripping canal while many other facilities have modified it to have a larger acceptance and a turbopump for stripping gas recirculation or completely removed it in order to increase transmission, especially for heavy ions [20,21]. Other facilities also have at their disposal an electrostatic quadrupole triplet immediately after the foil stripper to significantly limit the beam's emittance into the high energy column [22].

The 6 MV aluminum distribution yielded a mean charge state higher than the SG model predicted by 0.28. It also had the highest total transmission of the four isotopes measured. The transmission of the elemental $^{27}Al^{7+}$ beam at 6 MV was 5.2(2)%, 3–4 times lower than

Table 1
Table of different beams measured including their total transmission using both single and second foil stripping. Column SG refers to the predicted mean charge state given by the SG Model. The next two columns are the total particle transmission measured for each injected beam when using either only the terminal foil stripper ϵ_S, or both foil strippers ϵ_D as defined in Eqs. (11) & (12). R_T is defined in Eq. (13) and the text thereafter.

Terminal voltage (MV)	Isotope	Injection	υ_p (km/s)	Measured $\bar{q}$	SG $\bar{q}$	ϵ_S (%)	ϵ_D (%)	R_T
3	^{27}Al	$^{27}Al^-$	4687	5.56	4.90	4.3(12)	–	–
6	^{27}Al	$^{27}Al_2^-$	4658	5.33	4.87	4.4(12)	–	–
6	^{27}Al	$^{27}Al^-$	6587	6.63	6.35	13.5(4)	3.6(4)	0.51
6	^{56}Fe	$^{56}Fe^-$	4574	8.41	7.59	7.7(19)	5.8(14)	0.10
6	^{90}Zr	$^{90}ZrO^-$	3324	8.45	7.38	7.2(15)	0.169(4)	3.03
6	^{55}Mn	$^{55}MnO^-$	4062	7.14	6.76	2.15(5)	1.34(3)	0.034

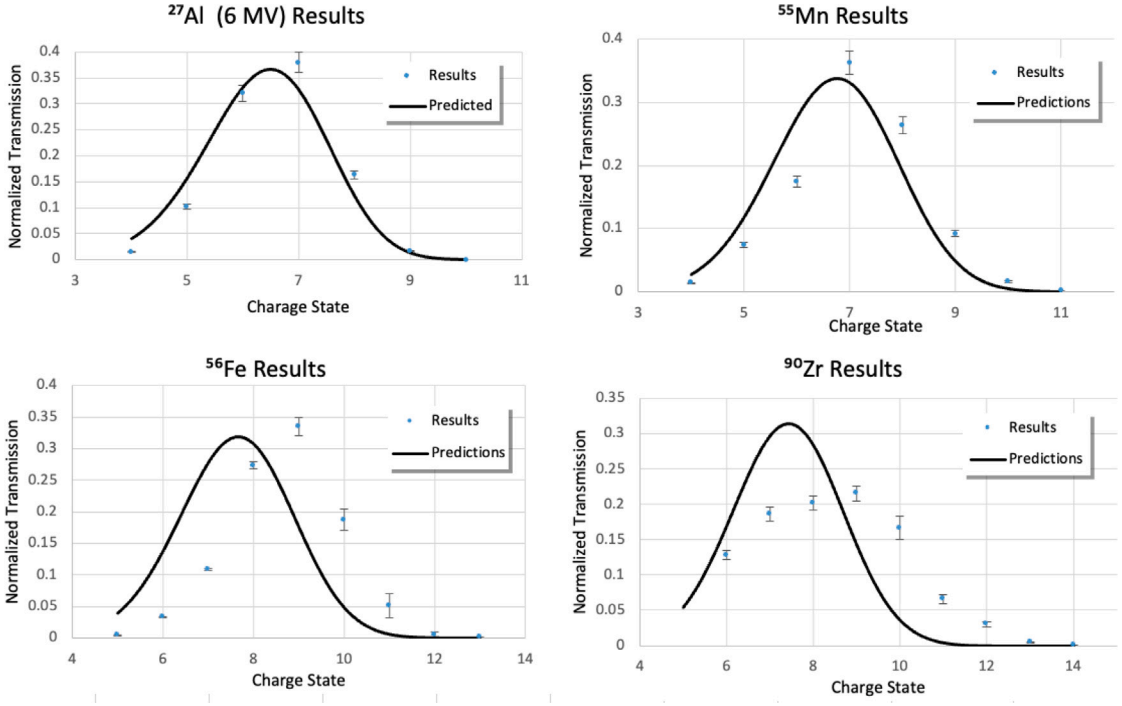

Fig. 2. Comparison of measured charge state distributions with their respective predictions using the model described in Section 2. The results are normalized to the single transmissions ϵ_S listed in Table 1. Aluminum and manganese both show good agreement with model predictions. Iron shows an appropriate shape, but the mean charge state is off by 0.82. Zirconium shows little agreement with predictions.

18% reported in [20], where a modified stripping canal increased the acceptance by a factor of 5. Likewise, 15% is reported for the transmission of the $^{27}Al^{7+}$ charge state in [19], where gas and foil stripping were both used and the 14UD accelerator was operated closer to its limit at 14.4 MV. While still lower, the results presented here are not unreasonable given these considerations. As expected, the transmission of the other two aluminum beams was worse. In both cases the stripped beam has a larger emittance than the 6 MV elemental beam, due to the lower potential causing less acceleration, or the coulomb explosion occurring after molecular dissociation. The dymer aluminum beam is predicted to have a similar distribution to the 3 MV Aluminum beam, as the velocities at the terminal are nearly identical and there is no dependency on mass in the model. This is experimentally confirmed, as the two distributions, shown in Fig. 3 are almost identical with their mean charge states differing by 0.23. The observed drop from 13.5(4)% to 4.4(12)% gives a rough estimate for how much the Coulomb explosion reduces the transmission, yielding a factor of 3 decrease (6 if only one atom is considered as it would be if this was a non-dymer molecular beam).

For manganese, the observed mean charge state was close to the predicted value, differing by 0.38. The lower charge states' transmissions were consistently lower than predicted, while the higher charge states had more transmission. This caused the overall shape of the distribution to match predictions, especially when considering the difference in the observed and predicted mean charge states. The total transmission of the manganese beam was the lowest, attributed to the Coulomb explosion from molecular dissociation in the stripper foil. The use of gas stripping for the molecular dissociation would help to limit this, but would have limited the capability of comparing to the model described in Section 2 as it only considers foil stripping. The measured transmission also showed the largest discrepancy when compared to other facilities. On a similar FN Tandem the $^{55}Mn^{10+}$ transmission was 6.5% at 9.28 MV terminal voltage that only uses foil stripping [18,23], and 9% for $^{53}Mn^{11+}$ on a 14UD tandem at 14.4 MV terminal voltage using a combination of gas and foil stripping and a electrostatic quadrupole triplet in the terminal [19].

The iron beam was the first to show significant deviation from the predicted mean charge state with the observed value being 0.82 higher than the value given by the SG model. The zirconium beam was the worst with a difference of 1.07. The shape of the iron distribution matched with predictions, however the width of the zirconium distribution was significantly larger. The results of the SG fit though deviate from the dataset used significantly in the mass region containing zirconium. Figure 3 of [10] suggests the mean charge state

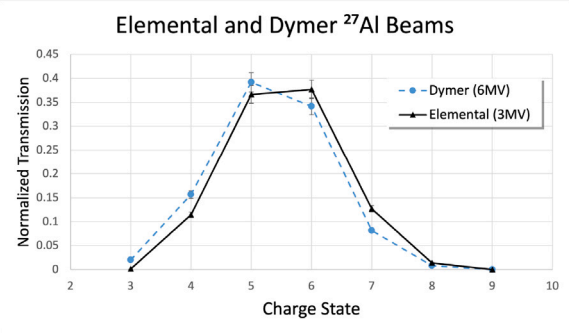

Fig. 3. Charge state distributions of an aluminum beam injected as dymer vs. elemental. The results are normalized to the single transmissions ϵ_S listed in Table 1. The terminal voltage is selected such that each beam has the same velocity upon reaching the terminal foil stripper. The distributions nearly overlap, showing that the charge state distribution is independent of any molecular dissociation required.

differs from the fit by more than 1 when the number of bound electrons $N_b = Z_p - \bar{q}_{exp}$ is similar to the value measured in this work of $N_b = 31.55$ for zirconium. This figure also highlights the M-shell closure, suggesting it corresponds to the increased deviation. Figure 4 in [10] has a spike in the experimentally determined distribution width for $N_b \in [30, 32]$ corresponding to the broader shape of the zirconium distribution measured here. The zirconium beam is also the only one where the limits of the analyzing magnet's rigidity prevented a full scan of the single foil stripping charge states. The total transmission is likely higher than that reported in Table 1 for zirconium and the value there instead corresponds to the transmission of charge states that were able to be measured. The measured transmission is lower when compared to [24] where 2.5–4.5% was observed on $^{92}Zr^{14+}$ at 14.15 MV in the 14UD tandem, however their transmission is improved with a quadrupole triplet following their foil stripper.

4.2. Second foil stripping results

For the evaluation of the second foil stripping method, 98 different measurements were performed across the four elements chosen. These results are shown in Fig. 4. Three of the four beams showed some charge state combinations that were more favorable than their single foil stripping counterparts. For example, the $^{55}Mn^{11+}$ beam had a transmission of 0.0039(4)% whereas the doubly stripped $^{55}Mn^{8+\rightarrow14+}$ beam had a transmission of 0.090(9)% while having the same energy and lower magnetic rigidity. This observation and other examples are shown in Table 2. Further measurements showed the $^{55}Mn^{10+}$ had a comparable transmission to the $^{55}Mn^{8+\rightarrow15+}$ yet the latter beam had 9 MeV more energy. The zirconium beam exhibited no such cases of either scenario due to the total second foil stripping transmission being lower than the total single foil stripping transmission due to excessive scattering losses. With the exception of the zirconium beam scattering losses at the second foil stripper were generally lower than what was lost at the terminal foil stripper, shown in the last column of 1. This shows that overall, the scattering losses are dampened at the second foil stripper due to the increased beam energy.

When compared to the predicted distributions, observations showed good agreement. In each case, the charge state distribution after single foil stripping yields a higher mean than predicted, as observed in the single foil stripping data. The final mean charge states however tend to be closer to the predicted values and, in the case of aluminum, even below. One possible explanation is the energy lost in the stripper foil, which was not factored into the predicted distributions. The energy loss here though is predicted to be 50 keV, amounting to a 0.1–0.7% difference. Another possibility is the shell effects that may present, especially as Z_p increases. This has been considered elsewhere as a possible reason for deviation [7,10,14].

Another effect of second foil stripping is the increase of produced beams with similar p/q values that would have a close enough rigidity to pass through an analyzing magnet. On this setup, with the transmission measured on the shutter Faraday cup, these interfering beams

Fig. 4. Observed second foil stripping charge state distributions and their predicted values. Each state was measured until the final beam current was imperceptible on the final Faraday cup. The observed dip in the $Zr^{10+\rightarrow15+}$ plot exhibited the same behavior upon remeasurement. The color scale denotes what fraction of the total transmission (ϵ_D defined in Eq. (12) and listed in Table 1) each state occupies.

Table 2
Table of examples where second foil stripping generated a beam with the same energy but higher transmission than single foil stripping. Values in the transmission columns reflect the particle transmission measured. The double state is the charge state after the terminal stripper foil followed by the charge state after the second foil stripper. The beam energy includes 70 keV from the ion source. The Gain column is the ratio of the Double Transmission and Single Transmission columns and is the increase in particle current observed when switching from single to double foil stripping.

Isotope	Single state	Single foil transmission (%)	Double state	Double foil transmission (%)	Beam energy (MeV)	Gain
^{27}Al	9+	0.24(2)	8+→10+	0.34(17)	60.07	1.4
^{55}Mn	10+	0.035(18)	8+→12+	0.092(9)	64.70	2.6
^{55}Mn	10+	0.035(18)	7+→13+	0.14(14)	64.70	4.0
^{55}Mn	11+	0.0039(4)	9+→13+	0.029(3)	70.70	7.4
^{55}Mn	11+	0.0039(4)	8+→14+	0.090(9)	70.70	23.1
^{55}Mn	11+	0.0039(4)	7+→15+	0.056(6)	70.70	14.4
^{56}Fe	11+	0.39(4)	9+→13+	0.44(5)	72.07	1.1
^{56}Fe	12+	0.034(3)	11+→13+	0.058(6)	78.07	1.7
^{56}Fe	12+	0.034(3)	10+→14+	0.31(3)	78.07	9.1
^{56}Fe	12+	0.034(3)	9+→15+	0.41(4)	78.07	12.1
^{56}Fe	12+	0.034(3)	8+→16+	0.13(14)	78.07	3.8

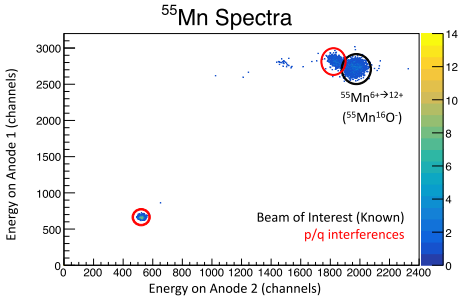

Fig. 5. Spectra for beams produced when set up for a $^{55}Mn^{6+\rightarrow12+}$ beam. A few distinct species can be seen, with their possible identity and injection molecule shown. The presence of multiple species highlight one of the additional challenges of second foil stripping.

would have also contributed to current readings before any filtering elements could have been used to isolate the beam of interest. An example of these contaminants in a manganese beam is shown in Fig. 5. While not every combination has these contaminants, they are more likely to occur when using the second foil stripper and were observed in a few of the beams of each element used. Two of the iron beams, the $^{56}Fe^{7+\rightarrow10+}$ and $^{56}Fe^{10+\rightarrow11+}$ ones, differed in magnetic rigidity by 0.016%. In this case, both beams were observed when parameters were selected for either one. This shows that in any experiment sensitive to multiple beam species, further filtering, such as with a Wien filter, would be necessary.

5. Conclusions and future work

Second foil stripping in tandem accelerators has been shown to be a useful technique for reaching higher energy beams. For the four different beams presented here, each case showed examples where second foil stripping yielded similar beam energies with higher abundances, or higher energy beams than single foil stripping was capable of producing. Despite the low observed transmissions, when compared to other facilities, the increase in transmission of the highest energy beams would be expected at any facility that aims to install a second foil stripper. In some cases a factor of 10–20 times more beam current was observed when using second foil stripping to generate a beam of the same energy as one using single foil stripping alone.

Comparisons to model predictions of charge state abundances showed fair agreement for each beam using terminal foil stripping alone with the largest discrepancy attributed to zirconium, however the data used to form the model was the least accurate in the region containing zirconium. In each case the measured mean charge state was found to be higher than predicted. When using second foil stripping, the observed most probable charge state combinations were in good agreement with what the SG model predicted.

This technique can be very useful to laboratories using a tandem accelerator for their prospective programs, specifically for experiments where the higher particle transmission leads to shorter counting times. The second foil stripper can also enable radioactive ion beam researchers to exploit a larger cross section in a reaction that is unreachable with current energies and also decrease the dispersion of any species produced in-flight as is the case in inverse kinematics measurements. It is been shown that this can be done with limited decreases in overall beam transmission, and in some cases, may even provide more beam to the final target. Retrofitting an existing tandem accelerator with such a system can be a difficult task, given the spatial limitations and new control systems required as well as characterizing the potential changes in ion optics. Such an undertaking should also be considered alongside the availability of access to other accelerator labs capable of higher energies. Nevertheless, it has been shown the limits in energy and transmission of such accelerators can be extended past their normal capabilities with the implementation and use of a second foil stripper.

CRediT authorship contribution statement

T.L. Bailey: Writing – review & editing, Writing – original draft, Visualization, Methodology, Investigation, Formal analysis, Data curation, Conceptualization. **L.K. Callahan:** Writing – review & editing, Methodology, Investigation, Data curation, Conceptualization. **A.M. Clark:** Writing – review & editing, Methodology, Investigation, Data curation, Conceptualization. **A.D. Nelson:** Writing – review & editing, Methodology, Investigation, Data curation, Conceptualization. **L. Wood:** Writing – review & editing, Visualization, Formal analysis, Data curation. **P. Collon:** Writing – review & editing, Supervision, Project administration, Methodology, Investigation, Funding acquisition, Conceptualization.

Declaration of competing interest

The authors declare that they have no known competing financial interests or personal relationships that could have appeared to influence the work reported in this paper.

Data availability

Data will be made available on request.

Acknowledgments

This work is supported by the National Science Foundation, USA Grant Nos. NSF PHY-2011890 and NSF PHY-2310059 and the Nuclear Regulatory Commission, USA Award No. 31310019M0037.

References

[1] Accelerators Around the World - National Electrostatics Corp., URL https://www.pelletron.com/library/accelerators-around-the-world/.
[2] D. Weisser, Stripper systems, in: R. Hellborg (Ed.), Electrostatic Accelerators: Fundamentals and Applications, Springer Berlin Heidelberg, Berlin, Heidelberg, 2005, pp. 166–180, http://dx.doi.org/10.1007/3-540-27095-7_16.
[3] K. Ostdiek, Measurement of the Half-Life of 60Fe for Stellar and Early Solar System Models Using the Direct Decay of 60mCo and Accelerator Mass Spectrometry (Ph.D. thesis), (July) University of Notre Dame, 2016.
[4] K.M. Ostdiek, T.S. Anderson, W.K. Bauder, M.R. Bowers, A.M. Clark, P. Collon, W. Lu, A.D. Nelson, D. Robertson, M. Skulski, R. Dressler, D. Schumann, J.P. Greene, W. Kutschera, M. Paul, Activity measurement of Fe 60 through the decay of Co 60 m and confirmation of its half-life, Phys. Rev. C 95 (5) (2017) 1–8, http://dx.doi.org/10.1103/PhysRevC.95.055809.
[5] T. Joy, Simulation of heavy ion scattering at strippers in beam optics calculations for tandem Van de Graaff accelerators, Nucl. Instrum. Methods 106 (2) (1973) 237–240, http://dx.doi.org/10.1016/0029-554X(73)90343-1.
[6] T. Bailey, A. Clark, L. Callahan, A. Nelson, M. Paul, M. Schiffer, D. Blankstein, P. Collon, Development towards 53mn Accelerator Mass Spectrometry capabilities at the University of Notre Dame, Nucl. Instrum. Methods Phys. Res. B 536 (2023) 1–6, http://dx.doi.org/10.1016/J.NIMB.2022.12.011.
[7] C.J. Schmitt, Equilibrium Charge State Distributions of Low-Z Ions Incident on Thin Self-Supporting Foils (Ph.D. thesis), University of Notre Dame, 2010, p. 135.
[8] J.F. Ziegler, The stopping and range of ions in solids, in: J.P. Biersack, U. Littmark (Eds.), in: Stopping and Ranges of Ions of Matter ; v. 1, Pergamon, New York, 1985.
[9] R. Sayer, Semi-empirical Formulas for Heavy-ions Stripping Data, URL https://www.osti.gov/servlets/purl/7284929-yHspNS/.
[10] G. Schiwietz, P.L. Grande, Improved charge-state formulas, Nucl. Instrum. Methods Phys. Res. B 175–177 (2001) 125–131, http://dx.doi.org/10.1016/S0168-583X(00)00583-8.
[11] G. Schiwietz, K. Czerski, M. Roth, F. Staufenbiel, P.L. Grande, Femtosecond dynamics – snapshots of the early ion-track evolution, Nucl. Instrum. Methods Phys. Res. B 225 (1–2) (2004) 4–26, http://dx.doi.org/10.1016/J.NIMB.2004.05.041.
[12] V.S. Nikolaev, I.S. Dmitriev, On the equilibrium charge distribution in heavy element ion beams, Phys. Lett. A 28 (4) (1968) 277–278, http://dx.doi.org/10.1016/0375-9601(68)90282-X.
[13] A.E. Stuchbery, A.N. Wilson, P.M. Davidson, Equilibrium charge-state distributions for S and Si ions emerging from iron and gadolinium targets with velocities near their K-shell electron velocity, Nucl. Instrum. Methods Phys. Res. B 243 (2) (2006) 265–271, http://dx.doi.org/10.1016/J.NIMB.2005.09.015.
[14] Y. Baudinet-Robinet, Equilibrium charge-state distributions of highly stripped ions in carbon foils, Nucl. Instrum. Methods Phys. Res. 190 (1) (1981) 197–202, http://dx.doi.org/10.1016/0029-554X(81)90221-4.
[15] K.X. To, R. Drouin, Etude des distributions des états de charge à l'équilibre d'ions énergétiques de bore dans le carbone et observation de niveaux d'énergie doublement excités du B III, Phys. Scr. 14 (6) (1976) 277, http://dx.doi.org/10.1088/0031-8949/14/6/006, https://iopscience.iop.org/article/10.1088/0031-8949/14/6/006, https://iopscience.iop.org/article/10.1088/0031-8949/14/6/006/meta.
[16] M. Skulski, T. Anderson, L. Callahan, A. Clark, A. Nelson, D. Robertson, E. Stech, P. Collon, Recent developments in the AMS system at the Nuclear Science Laboratory: Impacts on radionuclide sensitivities and current capabilities, Nucl. Instrum. Methods Phys. Res. B 488 (2021) 30–36, http://dx.doi.org/10.1016/j.nimb.2020.12.009.
[17] A.M. Clark, A.D. Nelson, T.L. Bailey, L.K. Callahan, A. Mazurek, P. Collon, Improvements for heavy-ion accelerator mass spectrometry at the university of Notre Dame ' s nuclear science laboratory, Nucl. Instrum. Methods Phys. Res. B 541 (April) (2023) 342–349, http://dx.doi.org/10.1016/j.nimb.2023.05.001.
[18] M. Schiffer, A. Dewald, C. Feuerstein, R. Altenkirch, A. Stolz, S. Heinze, A dedicated AMS setup for 53Mn/60Fe at the Cologne FN tandem accelerator, Nucl. Instrum. Methods Phys. Res. B 361 (2015) 95–99, http://dx.doi.org/10.1016/J.NIMB.2015.02.034.
[19] L.K. Fifield, S.G. Tims, T. Fujioka, W.T. Hoo, S.E. Everett, Accelerator mass spectrometry with the 14UD accelerator at the Australian National University, Nucl. Instrum. Methods Phys. Res. B 268 (7–8) (2010) 858–862, http://dx.doi.org/10.1016/J.NIMB.2009.10.049.
[20] G. Bonani, P. Eberhardt, H.J. Hofmann, T.R. Niklaus, M. Suter, H.A. Synal, W. Wölfli, Efficiency improvements with a new stripper design, Nucl. Instrum. Methods Phys. Res. B 52 (3–4) (1990) 338–344, http://dx.doi.org/10.1016/0168-583X(90)90433-U.
[21] M. Suter, J. Beer, D. Billeter, G. Bonani, H.J. Hofmann, H.A. Synal, W. Wölfli, Advances in AMS at Zurich, Nucl. Instrum. Methods Phys. Res. B 40–41 (PART 2) (1989) 734–740, http://dx.doi.org/10.1016/0168-583X(89)90466-7.
[22] L.K. Fifield, M. Suter, M.B. Froehlich, D. Koll, S. Pavetich, Z. Slavkovská, S.G. Tims, A. Wallner, Coulomb explosion of BeO- molecular ions – Revisited, Nucl. Instrum. Methods Phys. Res. B 538 (2023) 205–211, http://dx.doi.org/10.1016/J.NIMB.2023.03.006.
[23] M. Schiffer, R. Spanier, C. Müller-Gatermann, S. Herb, C. Feuerstein, G. Hackenberg, M. Marock, S. Heinze, A. Stolz, A. Dewald, S. Binnie, The first (53Mn/55Mn) isotopic ratio measurements at the Cologne FN-Tandem Accelerator, Nucl. Instrum. Methods Phys. Res. B 437 (2018) 87–92, http://dx.doi.org/10.1016/J.NIMB.2018.09.029.
[24] S. Pavetich, A. Carey, L.K. Fifield, M.B. Froehlich, S. Halfon, A. Kinast, M. Martschini, D. Nelson, M. Paul, A. Shor, J.H. Sterba, M. Tessler, S.G. Tims, L. Weissman, A. Wallner, 93Zr developments at the Heavy Ion Accelerator Facility at ANU, Nucl. Instrum. Methods Phys. Res. B 438 (2019) 77–83, http://dx.doi.org/10.1016/J.NIMB.2018.07.019.